2024, 21(3): 1086-1094
https://dx.doi.org/10.21123/bsj.2023.7904
P-ISSN: 2078-8665 - E-ISSN: 2411-7986
Baghdad Science Journal

Study the Structural Properties of Porous Silicon and their Applications as Thermal Sensors

Israa Akram Abbas *, Ameera J. Kadhm

Department of Physics, College of Education for Pure Science, Al-Mustansiriyah University, Iraq.
*Corresponding Author.

Received 07/10/2022, Revised 09/01/2023, Accepted 11/01/2023, Published Online First 20/08/2023, Published 01/03/2024

Abstract

The photo-electrochemical etching (PECE) method has been utilized to create pSi samples on n-type silicon wafers (Si). Using the etching time 12 and 22 min while maintaining the other parameters 10 mA/cm^2 current density and HF acid at 75% concentration.. The capacitance and resistance variation were studied as the temperature increased and decreased for prepared samples at frequencies 10 and 20 kHz. Using scanning electron microscopy (SEM), the bore width, depth, and porosity % were validated. The formation of porous silicon was confirmed by x-ray diffraction (XRD) patterns, the crystal size was decreased, and photoluminescence (PL) spectra revealed that the emission peaks were centered at 2θ of 28.5619° and 28.7644° for etching time 12 and 22 min, respectively. Studying the capacitance and resistivity during temperature increasing and decreasing for both itching times shows clearly that the prepared pSi as a thermal sensor is working better and in more selectivity for 20 min itching time.

Keywords: Porous silicon, Photoluminescence, Structural properties, Scanning electron microscopy, Thermal sensors.

Introduction

One of the most crucial concerns in measuring technology is thermal sensing. Thermal transducers have been manufactured and are being made in abundance[1]. Anisotropic etching is widely used in silicon bulk micromachining to produce microstructures for diverse applications in the field of microelectromechanical systems (MEMS). Furthermore, it is most commonly employed for surface texturing in order to reduce light reflection and hence improve the efficiency of crystalline silicon (c-Si) solar cells[2]. This approach has been used in industry for many years now. It provides a lot of benefits, but there are also some serious disadvantages, so it's important to look into alternatives. Many amazing characteristics of porous silicon (pSi) have been explored in-depth[1,2]. The pSi has a number of intriguing characteristics in addition to its photoluminescent properties, such as a variable index of refraction, low visible absorption of light, substantial interior surface, customizable surface chemistry, or strong chemical activity[3]. All of these characteristics, as well as the simple production of material and the ability to create precisely regulated multilayer structures, make it suitable for usage in a variety of industries, including optics, Opto- and microelectronics, biomedical applications, and chemical sensing[4,5]. The thermal conductivity of bulk crystalline Si follows the temperature dependence of single crystal dielectric materials. It is often regulated by phonon scattering with other phonons, Si isotopes, and crystal boundaries[6].

Paladiya and Kiani[7], discussed the impact of probe diameters on sensing performance is explored

2024, 21(3): 1086-1094
https://dx.doi.org/10.21123/bsj.2023.7904
P-ISSN: 2078-8665 - E-ISSN: 2411-7986
Baghdad Science Journal

in the context of several types of sensors used in diverse applications. Modifications to traditional procedures and the development of new technologies have enabled researchers to produce at the submicron and nanoscale levels. P. Ferrando-Villalba, et al.[8] showed that individual porous Si nanowires (NWs) produced from MACE have poor thermal conductivity (*K*), with values as low as 0.87 $Wm^{-1}K^{-1}$ for 90 nm diameter wires with 35 - 40% porosity. They establish a linear association with the NW diameter despite the significant suppression of long mean free path phonons in porous materials. Chen and Zhang[9] reported that the silicon material with aligned distributed rectangular-shaped holes is proposed for the manufacture of semiconductor devices. A comprehensive understanding the heat conduction is of great significance to improve the efficiency of thermoelectrical materials.

Baran et al.[10] discussed the effects of heat oxidation on the sensing characteristics of porous silicon. Electrochemical etching was used to create porous silicon substrates, which were then thermally oxidized at various temperatures. An EDS comparison reveals that porous surfaces oxidized at higher temperatures have greater oxygen-to-silicon ratios.

This work aimed to prepare porous silicon (pSi) using the PECE method and study the structural properties of porous silicon and discussed the results.

Materials and Methods

Experimental Work

The Formation of pSi

The materials and method used in the present study are n-type silicon (Si) wafer that is commercially available, 625 μ thick, with10 Ω. cm resistivities. The silicon wafer samples were cut as squares with dimensions of 1.5×1.5 cm^2. The samples were washed with ethanol to remove the impurities. To remove the natural oxide layer, they were etched in diluted 10% hydrofluoric (HF) acid. The PECE process was used to create the pSi layer in an electrolyte solution that was a 0.75:1 combination of 75% HF and 1% C_2H_5OH. Typically, ethanol is used to prevent the accumulation of hydrogen bubbles.

Teflon, which resists corrosion from the HF electrolyte exceptionally well, was used to construct the cell configuration. The sample is represented by the anode, which is situated halfway along the cell (Si). The cathode is shaped as a platinum (Pt) ring immersed in an HF electrolyte.

The (HF) electrolyte was poured into the Teflon cell's top. The electrolyte must be present in sufficient amounts to both covers the Pt electrode and provide the required fluorine ions. The laser IR source 810 nm was used to execute the PECE for 12 and 22 min at a current density of 20 mA/cm^2 with intensities ranging from 15 to 20 mW/cm^2. The typical schematic of the (PECE) system is illustrated in Fig.1.

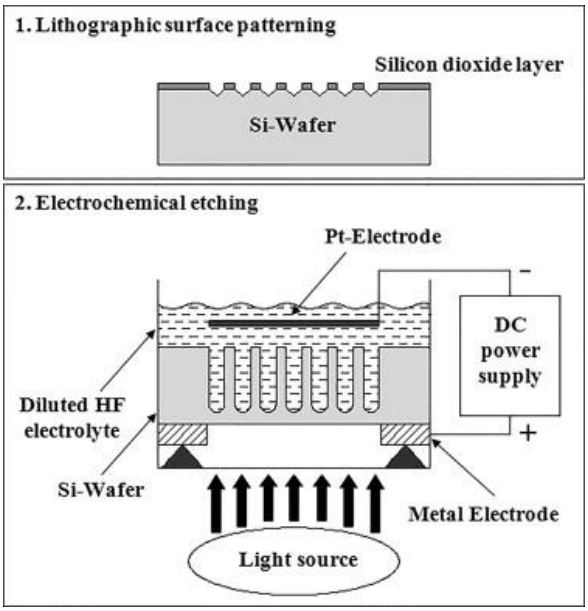

Figure 1. Schematic representation of the back-side illumination electrochemical etching technique[11].

Scanning Thermal Microscopy

The scanning Thermal Microscopy (SThM) method is depicted in Fig.2 as a thermal probe[12]. The thermosensitive Wollaston probe is used to perform thermal conductivity measurements. In order to precisely measure the probe's resistance, it is coupled to an electrical circuit using a Wheatstone bridge setup. The most popular way is to utilize a DC current to run the probe in what is known as the active mode [13,14]. The sample is placed far from the Wollaston wire, which, due to the Joule effect, is heated. After then, the electrical probe is powered

2024, 21(3): 1086-1094
https://dx.doi.org/10.21123/bsj.2023.7904
P-ISSN: 2078-8665 - E-ISSN: 2411-7986
Baghdad Science Journal

away from contact and the Wheatstone bridge is balanced. The sample is then in touch with the tip while still being at room temperature. The sample receives heat from the tip, causing the tip temperature to decrease and the electrical resistance to alter accordingly. This decrease in temperature affects the output voltage of the Wheatstone bridge and is directly related to the substance under investigation's thermal conductivity.

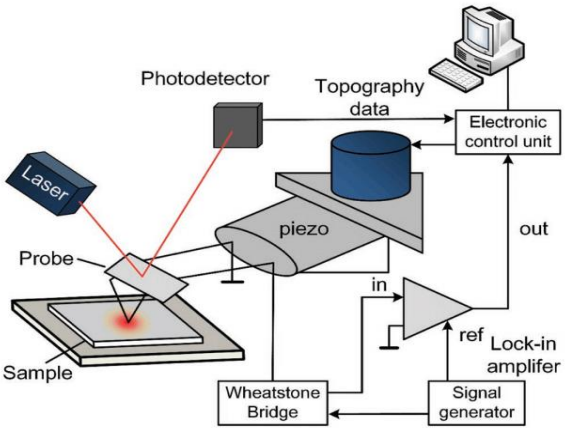

Figure 2. Schematic diagram of SThM setup[13].

Results and Discussion

XRD analysis

Analysis of XRD patterns was performed in the 2θ range of 10°-80° for (12 and 22)min etching time as shown in Figs.3,4 and their parameters in Table 1 of layers of c-Si and porous silicon.

These patterns, which has a modest, wider peak located between 28.5619° and 28.7644°, for etching times 12 and 22 min, respectively, compared with the standard value 28.352° as displayed in Table (1). Figs. 4, 5 confirm the development of pores on the surface of the crystalline silicon (c-Si). It also compares the XRD patterns of the c-Si to a slight widening and splitting peak of the porous silicon layer.

The values of d_{hkl} and 2θ are approximately equal to the standard values in the JCPDS standard card (JCPDS: 27-1402), as shown in Table 1. Using Eqs.1,2,3, 4 [15,16], it is possible to introduce the influence of etching time on crystalline size (C.S), the microstrain (ε), dislocation density (δ), number of crystallites per area (N_o), and β **is** has represented the full width at half maximum (FWHM) in degrees.

$$C.S = 0.9\lambda / \beta \cos\theta \quad \ldots\ldots\ldots \quad 1$$

$$\varepsilon = \beta / 4\cos\theta \quad \ldots\ldots\ldots \quad 2$$

$$\delta = 1 / (C.S)^2 \quad \ldots\ldots\ldots \quad 3$$

$$N_o = t / (C.S)^3 \quad \ldots\ldots\ldots \quad 4$$

The crystalline size (C.S) can be calculated by using the value of β from Figs. 2, 3 with the wavelength λ at broadening peak at the diffraction angle 28.5619 and 28.7644 for 12 min and 22 min, respectively. The crystalline size now can be determined by using equations 1 and 2 as 29.02 nm and 20.94 nm for 12 min and 22 min itching time, respectively. The microstrain (ε), dislocation density (δ), and number of crystallites per area (N_o) are calculated using Eqs.2, 3, 4, respectively.

Table 1. Parameters for the structures of C-Si and PS at various etching times.

Parameters	Etching time (min.)		Standard Values
	12	22	
2θ	28.5619	28.7644	28.352
d_{hkl}	0.31252	0.310374	0.31454
FWHM (β)	0.2952	0.4093	
C.S (nm)	29.02615	20.94402	…….
Microstrain (ε)	0.001248	0.001729	……
δ	0.00118	0.00227	
N_o	0.00049	0.00239	

2024, 21(3): 1086-1094
https://dx.doi.org/10.21123/bsj.2023.7904
P-ISSN: 2078-8665 - E-ISSN: 2411-7986
Baghdad Science Journal

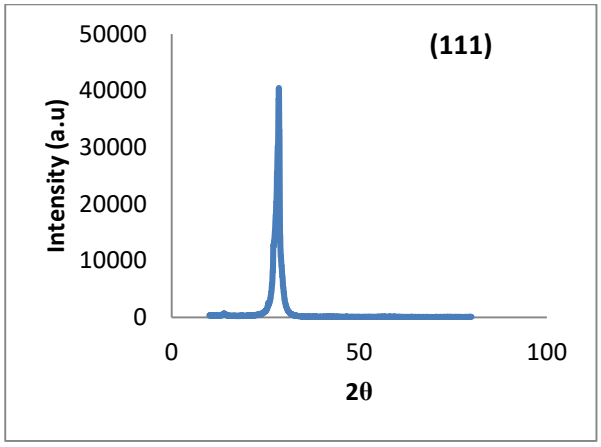

Figure 2. The XRD pattern of the sample prepared at 12 min etching time.

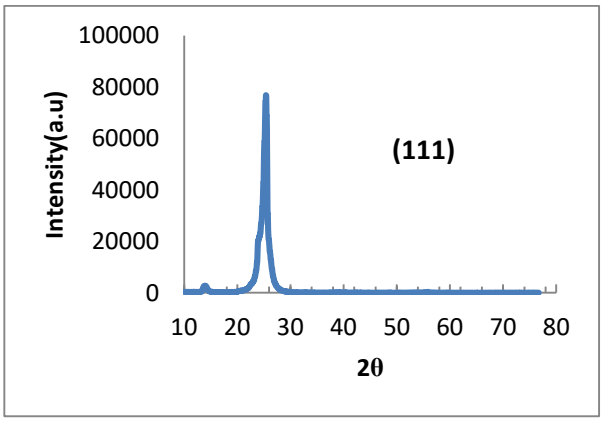

Figure 3. The XRD pattern of the sample prepared at 22 min etching time.

Field-Emission Scanning Electron Microscopy (FESEM)

The surface and cross-section images of porous silicon at various etching times are shown in Figs. 4 and 5. The images reveal that a layer of tiny nanoscale spheres with a diameter of about 50 nm covers the area of the pores and the outer surface layer.

The sample etched for 12 min appears to develop grooves and pores down to a depth of 12.82 μm. The formation of hexagonal holes with a depth of 12.82 μm and walls dividing the pore spaces were caused by lengthening the etching duration to 22 minutes. These structures were then covered with a layer of spherical nanoparticles with a diameter of about 37.22 nm.

A group of PS is displayed in a homogeneous pattern and structural pores in (FESEM) pictures, which supports the creation of uniform porous structures on silicon. the effects of a 22 -minute growth period on surface morphology.

Field emission scanning electron microscopy (FESEM) images showed that porous Si etched using the 12 min itching time has a higher porosity and density than porous Si etched using 22 min itching time. The atomic force microscopy results supported the FESEM results showing that porous Si etched using 12 min itching time has the highest surface roughness relative to the samples produced using the 22 min itching time. High resolution X-ray diffraction revealed that porous Si produced through 12 min itching time has the highest peak intensity out of the 22 min itching time suggesting an improvement in pore uniformity with better crystalline quality.

The pores in the P-Si are seen as dark dots in Fig.3, the diameter of pSi increases with time in Fig.4. This largeness of width increases in holes number on the surface of pSi with etching time. After irradiation, Fig.4 shows a pore-like spherical shape elongated and the defect clusters of pSi samples were large than those of the samples before irradiation as in Fig.3, also, pore width was increased with increasing etching time, since the radiation reduces the thin walls between neighbour pores as Fig.4.

Fig. 6 depicts the EDX elemental analysis for porous silicon prepared at various times. In addition to the Au peak, their patterns show silicon and oxygen emission lines. The intensities of the peaks differ in their height depending on their presence ratio in the samples, with the oxygen peak growing while the silicon peak decreasing with increasing etching time, showing the oxidation of some silicon atoms during the etching process.

2024, 21(3): 1086-1094
https://dx.doi.org/10.21123/bsj.2023.7904
P-ISSN: 2078-8665 - E-ISSN: 2411-7986
Baghdad Science Journal

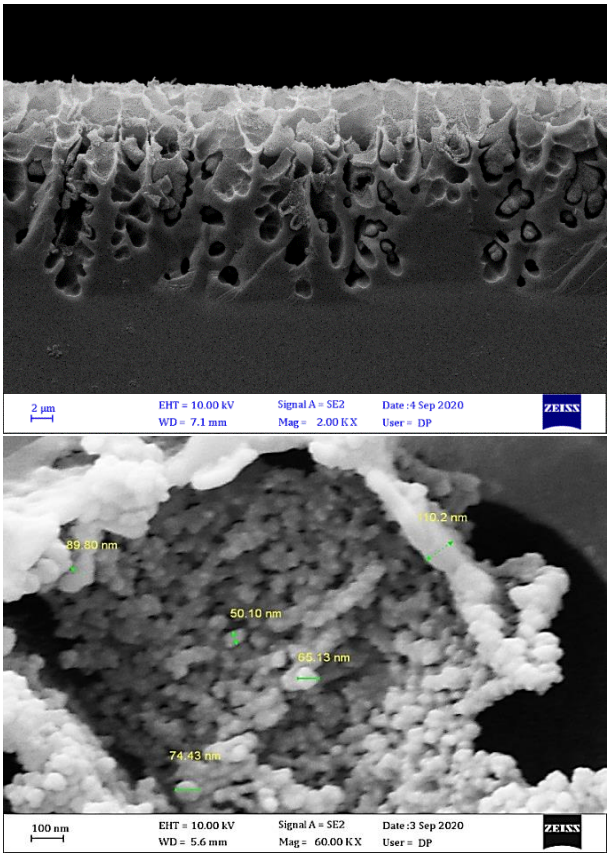

Figure 4. FE-SEM images at 60 KX of n-type pSi (111) produced at 12 etching time.

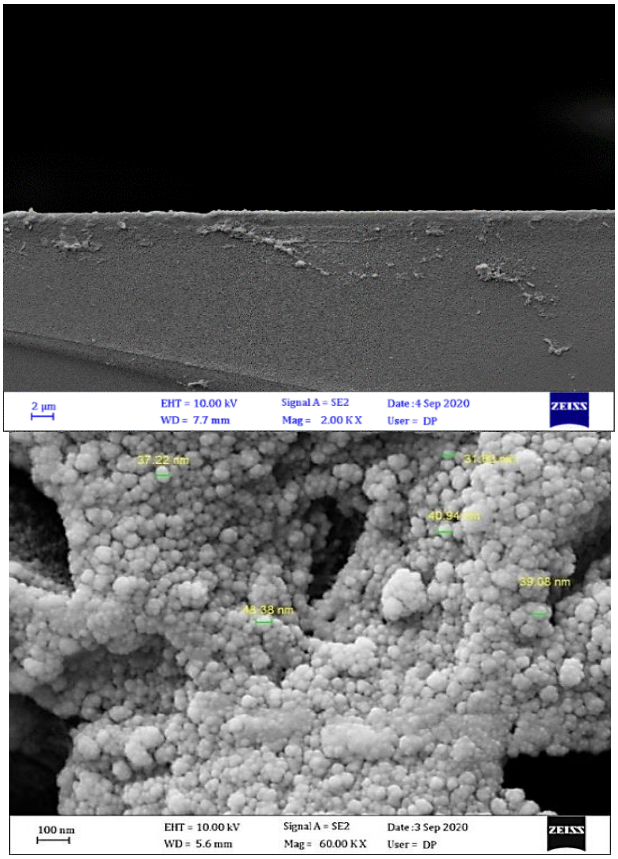

Figure 5. FE-SEM images at 60 KX of n-type pSi (111) produced at 22 etching time.

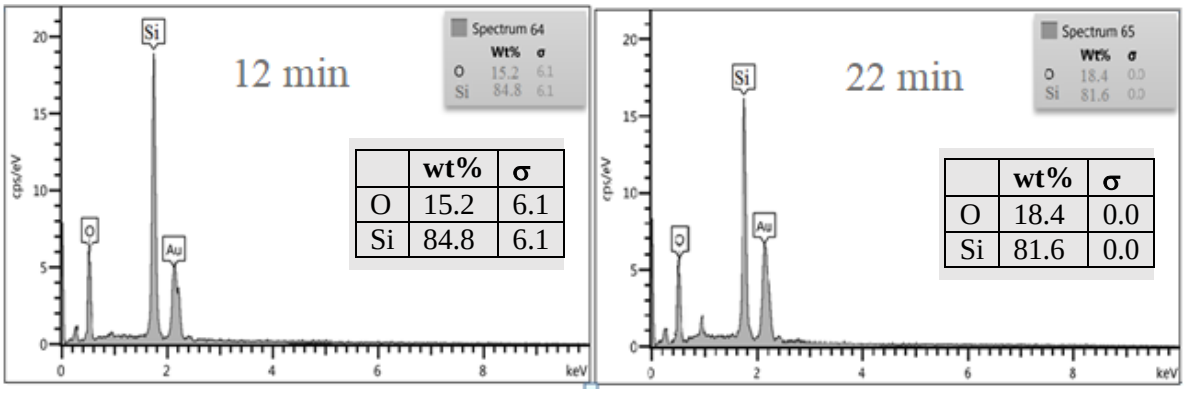

	wt%	σ
O	15.2	6.1
Si	84.8	6.1

	wt%	σ
O	18.4	0.0
Si	81.6	0.0

Figure 6. EDX spectra for porous silicon samples prepared at different etching time.

Thermal sensor

The response of the capacitance for the sensor shown in Fig.7 for the 12 min etched samples were recorded during the increasing and decreasing of the measured temperature with constant frequency at 10 kHz. Panel (A) from Fig. 7 shows that the capacitance is decreasing linearly with increasing temperature and panel (B) shows that the capacitance is decreasing with decreasing temperature as curvature variation. This means that the prepared pSi sample is very sensitive to temperature changes.

The sensor resistance was also recorded and displayed in Fig.8 with increasing and decreasing temperatures for the constant frequency at 20 KHz. The resistance is increasing steadily as the measured temperature is increasing as shown in panel (A) and also increases up to the temperature of

2024, 21(3): 1086-1094
https://dx.doi.org/10.21123/bsj.2023.7904
P-ISSN: 2078-8665 - E-ISSN: 2411-7986
Baghdad Science Journal

80 °C then steadily increases up to 100 °C and drops at the temperature of 110 °C.

The capacitance and resistance variation with time for the 22min etched sample was studied and plotted as a function of temperature as depicted in panels (A) and (B) of Figs. 9, 10.

The folk of the peaks around the measured temperature of 50 °C for the resistance while the measured temperature is decreasing means that the thermal sensor is more sensitive to the temperature of the sample etched at 22 min.

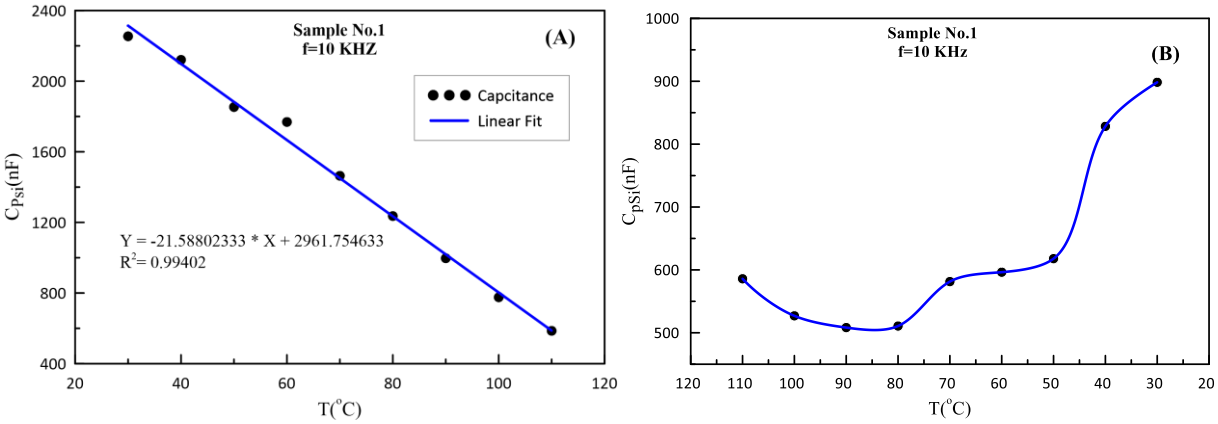

Figure 7. Capacitance variation with (A) increasing temperature and (B) decreasing temperature, for 12 min etched sample.

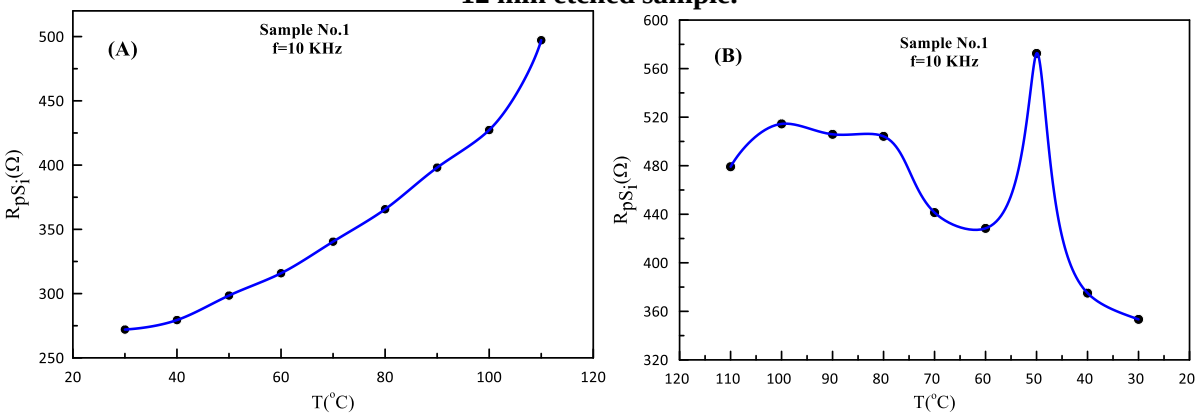

Figure 8. Resistance variation with (A) increasing temperature and (B) decreasing temperature, for 12 min etched sample.

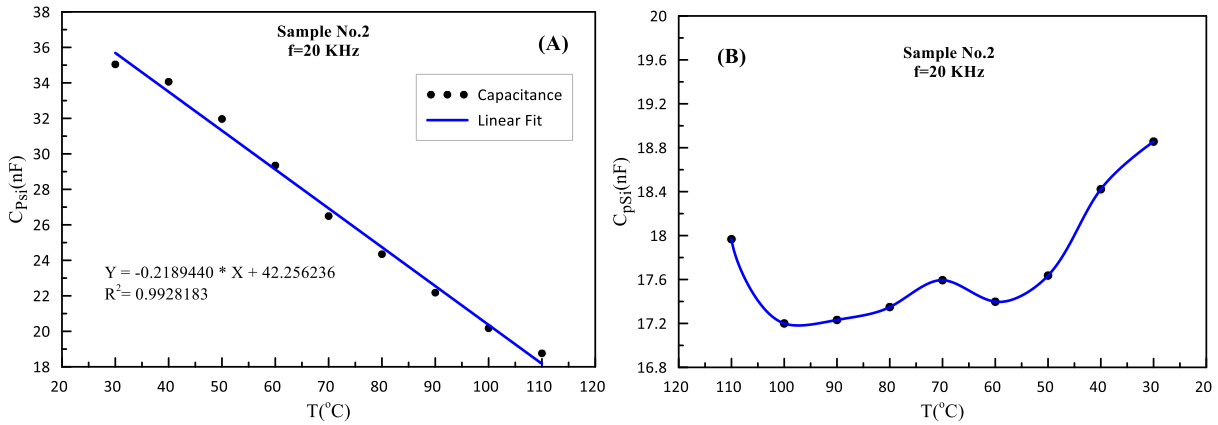

Figure 9. Capacitance variation with (A) increasing temperature and (B) decreasing temperature, for 22 min etched sample.

2024, 21(3): 1086-1094
https://dx.doi.org/10.21123/bsj.2023.7904
P-ISSN: 2078-8665 - E-ISSN: 2411-7986
Baghdad Science Journal

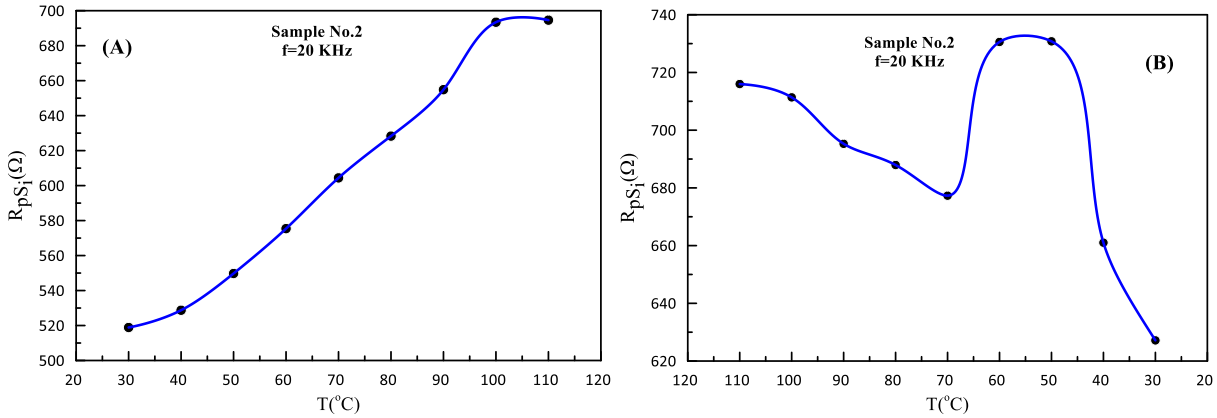

Figure 10. Resistance variation with (A) increasing temperature and (B) decreasing temperature, for 22 min etched sample.

Conclusion

In this study, the porous silicon (pSi) is prepared by the photo-electrochemical etching (PECE) method. The etching time is taken 12 min and 22 min for the preparation of pSi. The XRD analysis shows that when the etching current density increased the photoluminescence peak shifted toward shorter wavelengths which can be attributed to the changes in porous morphology Photoluminescence study showed that the emission peaks centred at approximately 20– 40 nm. The XRD analysis and SEM images and study of the resistivity and capacity variation with the measured temperature show that the porous silicon prepared with 22 min itching time is more adequate as a thermal sensor than the porous silicon prepared with 12 min itching time.

Acknowledgment

The Authors are very grateful for the support from department of Physics, College of Education for Pure Science, Al-Mustansiriyah University, Iraq.

Author's Declaration

- Conflicts of Interest: None.
- We hereby confirm that all the Figures and Tables in the manuscript are ours. Furthermore, any Figures and images, that are not ours, have been included with the necessary permission for re-publication, which is attached to the manuscript.
- Ethical Clearance: The project was approved by the local ethical committee in Al-Mustansiriyah University.

Author's Contribution Statement

The authorship of the title above certifies that they have participated in different roles as follows: The author I.A. A. Collecting the literature survey and help in preparation of pSi samples and made them ready for measurements and the author A. J. K. Preform the measurements of XRD and SEM and resistivity and capacity measurements and plotted the graphs and finally both of them contribute equally in writing the manuscript and made it ready for submission.

References

1. Sun P, Xu P, Zhu K, Zhu Z, Zhou Z. Silicon-Based optoelectronics enhanced by hybrid plasmon polaritons: bridging dielectric photonics and nanoplasmonics. Photonics 2021; 8 (11):482. https://doi.org/10.3390/photonics8110482.
2. Gonçales VR, Lian J, Gautam S, Tilley RD, Gooding JJ. Functionalized silicon electrodes in electrochemistry. Ann Rev Anal Chem. 2020; 13:135-58. https://doi.org/10.1146/annurev-anchem-091619-092506.

3. Ghanta U, Ray M, Biswas S, Sardar S, Maji TK, Pal SK, Bandyopadhyay NR, Liu B, Hossain SM. Effect of phonon confinement on photoluminescence from colloidal silicon nanostructures. J Lumin. 2018; 201:338-44. https://doi.org/10.1016/j.jlumin.2018.04.052.
4. Harb NH, Mutlak FA. Effect of etching current density on spectroscopic, structural and electrical properties of porous silicon photodetector. Optik. 2022; 249: 168298. https://doi.org/10.1016/j.ijleo.2021.168298.
5. Shang Y, Zhang L, Qi H, Wu Y, Zhang Y, Chen J. Study on Silicon Microstructure Processing Technology Based on Porous Silicon. In J Phys Conf. 2018. 986 (1): 012006. https://doi.org/10.1088/1742-6596/986/1/012006.
6. Ali SM, Alwan AM, Abbas OA. Influence of Laser Irradiation Times on Properties of Porous Silicon. Baghdad Sci J. 2007; 4(4): 640-5. https://doi.org/10.21123/bsj.2007.4.4.640-646.
7. Paladiya C, Kiani A. Nano structured sensing surface: Significance in sensor fabrication. Sens. Actuators B Chem. 2018; 268: 494-511. https://doi.org/10.1016/j.snb.2018.04.085.
8. Ferrando-Villalba P, D'Ortenzi L, Dalkiranis GG, Cara E, Lopeandia AF, Abad L, Rurali R, Cartoixà X, et al. Impact of pore anisotropy on the thermal conductivity of porous Si nanowires. Sci Rep 2018; 8(1): 1-9. https://doi.org/10.1038/s41598-018-30223-0.
9. Chen J, Zhang X. Pore-size dependence of the heat conduction in porous silicon and phonon spectral energy density analysis. Phys Lett A. 2020; 384(21): 126503. https://doi.org/10.1016/j.physleta.2020.126503.
10. Baran N, Renka S, Raić M, Ristić D, Ivanda M. Effects of Thermal Oxidation on Sensing Properties of Porous Silicon. Chemosensors. 2022; 10(9): 349. https://doi.org/10.3390/chemosensors10090349.
11. Rudawska A. Surface treatment in bonding technology. Academic Press; 2019. https://www.elsevier.com/books/surface-treatment-in-bonding-technology/rudawska/978-0-12-817010-6.
12. Gomès S, Assy A, Chapuis PO. Scanning thermal microscopy: A review. Phys. Status Solidi (a). 2015 Mar;212(3): 477-94. https://doi.org/10.1002/pssa.201400360.
13. Zhang Y, Zhu W, Hui F, Lanza M, Borca-Tasciuc T, Muñoz Rojo M. A review on principles and applications of scanning thermal microscopy (SThM). Advanced functional materials. 2020 May; 30(18): 1900892. https://doi.org/10.1002/pssa.201400360.
14. Jebril NM. Novel use of XRF in the adsorption processes for the direct analysis of cadmium and silver in absorbent Na-alginate beads. Baghdad Sci J. 2020; 17: 1139-1144. https://doi.org/10.21123/bsj.2020.17.4.1139.
15. Ajar SH, Ahmad EY, Hussein EA, Habib AA. Study the Effect of Irradiation on Structural and Optical Properties of (CdO) Thin Films that Prepared by Spray Pyrolysis. Ibn AL-Haitham J Pure Appl Sci. 2017 Mar 16; 28(2): 41-51. https://jih.uobaghdad.edu.iq/index.php/j/article/view/175/145.
16. Smilgies DM. Scherrer grain-size analysis adapted to grazing-incidence scattering with area detectors. J appl Crystallogr. 2009; 42(6): 1030-4. https://doi.org/10.1107%2FS0021889809040126.

2024, 21(3): 1086-1094
https://dx.doi.org/10.21123/bsj.2023.7904
P-ISSN: 2078-8665 - E-ISSN: 2411-7986
Baghdad Science Journal

دراسة الخصائص التركيبية للسيليكون المسامي وتطبيقاتها كأجهزة استشعار حرارية

اسراء اكرم عباس، أميرة جواد كاظم

قسم الفيزياء ، كلية التربية للعلوم الصرفة ، الجامعة المستنصرية ، العراق
.

الخلاصة

تم استخدام طريقة الحفر الضوئي الكهروكيميائي (PECE) لإنشاء عينات pSi على رقائق السيليكون من النوع n (Si). بأستخدام وقت الحفر (12 و 22 دقيقة) في التجربة مع الحفاظ على المعلمات الأخرى (10 ملي أمبير / سم^2 كثافة التيار وحمض HF بتركيز 75٪). تمت دراسة تغير السعة والمقاومة مع زيادة درجة الحرارة وانخفاضها للعينات المحضرة عند ترددات 10 و 20 كيلو هرتز. ، تم التحقق من صحة عرض المسام والعمق والمسامية باستخدام الفحص المجهري الإلكتروني (SEM). تم تأكيد تكوين السيليكون المسامي من خلال أنماط حيود الأشعة السينية (XRD) ، وأنخفض حجم البلورة ، وكشفت أطياف التلألؤ الضوئي (PL) أن قمم الانبعاث تركزت عند 2θ من 28.5619 ° و 28.7644 ° لوقت حفر 12 و 22 دقيقة على التوالي. تظهر دراسة السعة والمقاومة أثناء زيادة درجة الحرارة وانخفاضها لكلتا أوقات الحكة بوضوح أن pSi المحضر كمستشعر حراري يعمل بشكل أفضل وبانتقائية أكثر لمدة 20 دقيقة من وقت الحفر.

الكلمات المفتاحية: سيليكون مسامي ، تلألؤ ضوئي، الخصائص التركيبية، المسح المجهري الإلكتروني، مجسات حرارية